J. Fluid Mech. (1996), *vol.* 310, *pp.* 89–111

Unsteady tube flow over an expansion

By GIANNI PEDRIZZETTI

Dipartimento Ingengneria Civile, Università di Firenze. Via Santa Marta 3, 50139 Firenze, Italy

(Received 25 May 1995 and in revised form 21 August 1995)

Unsteady flow in a circular conduit with a smooth expansion is studied in detail by numerical integration of the equation of motion in the axisymmetric approximation. The values of governing parameters are chosen to be relevant to medical problems, and the geometry corresponds to a scenario of post-surgical conditions. The flow determined by an oscillatory volume is characterized by a sequence of vortex rings moving in the expanded part of the tube. The development of wall shear stress is governed by the separated translating vorticity which induces an evolving band of large intensity for about a complete oscillation cycle. This influences the dynamics of unsteady separation whose space–time development has revealed features of some generality which have been classified. The time variation of the pressure jump is dominated by inertial effects. The dependence of the details of the flow on the dimensionless parameters has been investigated systematically. The results obtained here have been compared with experimental and numerical studies of similar problems, similarities have been pointed out and differences discussed. Finally, the relevance of these results to physiological applications has been quantified by simulating the flow induced by a pulsatile flow rate.

1. Introduction

The understanding of unsteady motion in close conduits is currently receiving considerable attention because of its interest in many branches of engineering and in environment-related subjects including, in particular, biomechanics. In addition to the practical interest, previous investigations have shown how unsteadiness can lead to complex phenomena, even in simple external conditions, which are of intrinsic theoretical importance.

The key feature is the nonlinear behaviour of the separated vorticity. Once a vortex is separated it drastically changes the otherwise linear (in a loose sense) dynamics, modifies the boundary layer evolution and its separation, and eventually the whole flow. This phenomenology is equally present in both internal and external flows in similar basic ways even though its nonlinearity makes comparison possible only among very similar conditions.

The basic mechanics of vortex-induced boundary layer separation has been explored in several detailed studies (see, as recent examples, Ersoy & Walker 1987; Peridier, Smith & Walker 1991; Pedrizzetti 1992; and references therein) which are focused on the unsteady structure of the boundary layer up to separation. In external flows, rich dynamical patterns have been uncovered in geometrically simple cases like a two-dimensional oscillatory flow around a circular cylinder (Tatsuno & Bearman 1990; Justensen 1991; Nakano & Rockwell 1994; and references therein) and, more recently, important nonlinearities have been described for axisymmetric oscillating flow over a sphere (Mei & Adrian 1992; Chang & Maxey 1994). Still in external flows, oscillations

over a wavy wall (Blondeaux & Vittori 1991*a*) have been shown to be governed by the dynamics of separated vorticity.

The present work deals with the unsteady laminar flow inside a circular tube with a smooth expansion. The problem has relevance in many technical applications, and this study has been stimulated by discussions with the cardiovascular surgery community. Detailed description of the flow field can help the search for an explanation, in terms of incompressible fluid dynamics over rigid walls, of the post-surgical complications occurring in some carotid operations.

The study of oscillating laminar flow over an expansion has developed significantly in the last decade. The greater part of these analyses deals with sudden expansions in the form of a step but the global behaviour, as will be shown below, does not differ drastically from this until a smooth expansion is able to produce a significant separated flow. The present work considers an axisymmetric approximation of the flow whereas most studies have dealt with two-dimensional models (Sobey 1985; Tutty & Pedley 1993). These studies found the development of a train of waves, which can be defined as vortex waves, downstream of the step. They are related to the deflection of the oncoming vorticity which causes secondary separation alternating on the two opposite walls. The length and intensity of the wave region is related to the various flow parameters (Tutty & Pedley 1993); nevertheless this phenomenon appears quite general and has been found in different conditions such as pulsatile flow over a partially obstructed channel (Tutty 1992), and in channel flows perturbed by a moving indentation (Pedley & Stephanoff 1985; Ralph & Pedley 1988, 1989).

Oscillatory axisymmetric flow was studied numerically and experimentally by Ralph (1986, 1988) for the case of wavy-walled tubes. In that case, the flow development depends on the longitudinal length scale given by the wall- non-uniformity wavelength which interacts with the flow oscillation longitudinal length inducing resonance when these are comparable (Ralph 1986). On the other hand, in the present case no external length scale can interact with the oscillation amplitude.

The principal aim of the present work is to provide a detailed analysis of the flow through an expansion in a circular vessel. The study is carried out by numerical integration of the Navier–Stokes equation in the axisymmetric approximation. Even though this study is principally theoretical, it was stimulated by the hope of contributing to understanding some situations of the post-surgical carotid fluid dynamical state. For this reason, the choice of the expansion shape has been chosen to be that of an operated human carotid; also the value and the variation of the flow parameters have been chosen in similar way. Nevertheless many differences with the actual problem remain and the problem is strongly idealized to permit an easier theoretical investigation.

In §2 the fluid dynamical problem is formulated and in §3 the numerical technique is presented. The flow resulting from an imposed oscillatory flow rate is analysed in §4 for a reference set of parameters value, and in §5 the influence of variations of the parameters is explored. In §6 the flow rate is assumed as pulsatile with the shape of the pulsation taken from medical measurements, and the results are compared with the purely oscillatory case. Discussions are developed through the paper as results are reported; a concluding discussion is reported in §7.

2. Mathematical definition of the physical problem

Consider a tube with rectilinear axis and circular cross-section whose radius varies along the axis, and an incompressible viscous fluid, with density ρ and kinematic viscosity ν, moving inside it transporting an instantaneous volume flow rate which is

periodic in time with period T. Call R_0 the value of the radius of the tube infinitely far upstream where the section becomes uniform, and call U_0 the maximum value, in the period, of the velocity averaged over the section of radius R_0. Indicating with an asterisk the dimensional variables, the flow rate and the pipe radius are given by

$$Q^*(t^*) = \pi R_0^2 U_0 f(t^*/T), \quad R^*(x^*) = R_0 R(x^*/R_0), \tag{1}$$

where x^* is a coordinate coincident with the tube axis, and t^* is the time.

We choose the period T and the radius R_0 as the units of time and length, respectively. The dimensionless radius of the tube is given by $R(x)$, and the dimensionless mean velocity infinitely far upstream is given by

$$U(t) = K_c f(t), \tag{2}$$

where K_c is the Keulegan–Carpenter number defined as

$$K_c = U_0 T/R_0; \tag{3}$$

this is used in preference to the Strouhal number which is defined as its inverse.

Assume the duct axis to be the x-axis of a cylindrical system of coordinates $\{x, r, \theta\}$; the approximation of axial symmetry makes the flow independent of the θ-coordinate. The governing equations are the axisymmetric form of the Navier–Stokes equations which are written in the vorticity–streamfunction formulation as

$$\frac{\partial \omega}{\partial t} + \frac{1}{r}\frac{\partial \psi}{\partial r}\frac{\partial \omega}{\partial x} - \frac{1}{r}\frac{\partial \psi}{\partial x}\frac{\partial \omega}{\partial r} + \frac{\omega}{r^2}\frac{\partial \psi}{\partial x} = \frac{1}{\alpha^2}\left(\frac{\partial^2 \omega}{\partial x^2} + \frac{\partial^2 \omega}{\partial r^2} + \frac{1}{r}\frac{\partial \omega}{\partial r} - \frac{\omega}{r^2}\right), \tag{4}$$

where $\omega(x, r, t)$ is the azimuthal vorticity and $\psi(x, r, t)$ is the Stokes streamfunction; the parameter α^2 is the inverse of the dimensionless viscosity, defined as

$$\alpha^2 = \frac{R_0^2}{\nu T}, \tag{5}$$

and is often referred as the Stokes number (α is also known as the Womersley number).

The vorticity and streamfunction are related by the Poisson equation

$$-\omega r = \frac{\partial^2 \psi}{\partial x^2} + \frac{\partial^2 \psi}{\partial r^2} - \frac{1}{r}\frac{\partial \psi}{\partial r}; \tag{6}$$

the velocity field, automatically satisfying the continuity equation, can be computed from the streamfunction (Batchelor 1967).

Equations (4) and (6) must be completed with boundary conditions. Infinitely far upstream and downstream, where the tube section tends to be uniform, the flow is assumed to be uniform as well. On the axis of the duct, $r = 0$, the boundary conditions are given by symmetry considerations, resulting in

$$\omega = 0, \quad \psi = 0 \quad \text{at} \quad r = 0. \tag{7}$$

At the wall of the tube the velocity vector must vanish. A zero value for the normal velocity implies that the streamfunction is constant along the wall and is proportional to the instantaneous discharge flowing in the tube (Batchelor 1967). The other condition of no tangential velocity gives the further constraint that the first-order normal derivative of the streamfunction and the second-order mixed derivative are zero. These, with the aid of equation (6), specify the value of the wall vorticity. The boundary conditions at the wall can be better expressed by choosing a system of coordinates where the wall coincides with a constant coordinate curve.

We apply a shearing coordinate transformation (Eiseman 1985; Ralph 1986) replacing the r-coordinate with a new z-coordinate by defining

$$r = zR(x); \tag{8}$$

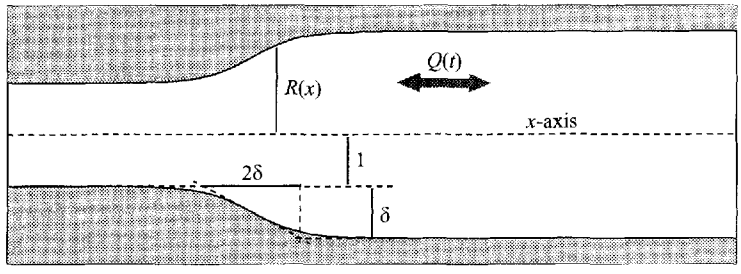

FIGURE 1. Sketch of the tube geometry (dimensionless).

the new system of coordinates $\{x, z\}$ is non-orthogonal and is well suited only to a slowly varying boundary (a suggested upper limited is 60°); on the other hand it has a wide generality and its use can also be extended to boundaries given only numerically and so to evolving boundaries. The Poisson equation (6) is now written as

$$-\omega r = \frac{\partial^2\psi}{\partial x^2} + \left[\left(\frac{\partial z}{\partial x}\right)^2 + \left(\frac{\partial z}{\partial r}\right)^2\right]\frac{\partial^2\psi}{\partial z^2} + 2\frac{\partial z}{\partial x}\frac{\partial^2\psi}{\partial x z} + \left[\frac{\partial^2 z}{\partial x^2} - \frac{1}{r}\frac{\partial z}{\partial r}\right]\frac{\partial\psi}{\partial z}, \tag{9}$$

and the equation of motion (4) can be expressed, formally, in the manner

$$\frac{\partial\omega}{\partial t} = -\mathscr{J}(\omega,\psi) - \mathscr{K}(\omega,\psi) + \frac{1}{\alpha^2}\mathscr{D}(\omega). \tag{10}$$

where the operators $\mathscr{J}, \mathscr{K}, \mathscr{D}$ represent the Jacobian term, the additional nonlinear term related to axial symmetry, and the diffusive term respectively. These are given by

$$\left.\begin{aligned}
\mathscr{J} &= \frac{1}{r}\frac{\partial z}{\partial r}\left(\frac{\partial\omega}{\partial x}\frac{\partial\psi}{\partial z} - \frac{\partial\psi}{\partial x}\frac{\partial\omega}{\partial z}\right),\\
\mathscr{K} &= \frac{\omega}{r^2}\left(\frac{\partial\psi}{\partial x} + \frac{\partial z}{\partial x}\frac{\partial\psi}{\partial z}\right),\\
\mathscr{D} &= \frac{\partial^2\omega}{\partial x^2} + \left[\left(\frac{\partial z}{\partial x}\right)^2 + \left(\frac{\partial z}{\partial r}\right)^2\right]\frac{\partial^2\omega}{\partial z^2} + 2\frac{\partial z}{\partial x}\frac{\partial^2\omega}{\partial x z} + \left[\frac{\partial^2 z}{\partial x^2} + \frac{1}{r}\frac{\partial z}{\partial r}\right]\frac{\partial\omega}{\partial z} - \frac{\omega}{r^2}.
\end{aligned}\right\} \tag{11}$$

The new coordinates permit the easier introduction of the boundary conditions at $z = 1$ which become

$$\psi(x, z = 1, t) = \tfrac{1}{2}K_c f(t), \tag{12}$$

$$\omega(x, z = 1, t) = -R^{-3}\left(1 + \left(\frac{\mathrm{d}R}{\mathrm{d}x}\right)^2\right)\frac{\partial^2\psi}{\partial z^2}\bigg|_{z=1}. \tag{13}$$

The physical problem is determined by the numerical values of the dimensionless parameters K_c and α^2, and by the shape of the functions $f(t)$ and $R(x)$. These quantities have been determined by referring to the post-surgical carotid fluid dynamical state. By fitting a relevant number of actual measurements (about 15), it has been found that the wall profile

$$R(x) = 1 + \frac{\delta}{2}\left(1 + \tanh\frac{x}{\delta}\right) \tag{14}$$

is a one-parameter family which represents a good approximation of real situations, where the parameter δ is, typically, around unity. A sketch of the typical geometry is given in figure 1. The flow rate is assumed sinusoidal

$$f(t) = \sin(2\pi t), \tag{15}$$

because of its theoretical importance in the understanding of unsteady flows; in §6 a different, pulsatile, unsteadiness will be considered for completeness. The Keulegan–Carpenter number ranges approximately from 20 to 100, and the Stokes number from 2 to 15. A reference case, corresponding to $K_c = 50$, $\alpha^2 = 6$, $\delta = 1$, will be analysed in detail first, then the parameters will be varied around this reference set and the various results compared.

3. Numerical method

The first step in building a numerical model is given by the definition of a finite computational grid to be superimposed over the physical domain. The present problem is dominated by the vorticity separated from the boundary layer and a higher resolution is required close to the wall. For this reason we introduce a stretching of the z-axis by defining a new coordinate ζ by

$$z = \frac{\tanh(a\zeta)}{\tanh(a)}, \tag{16}$$

where a is a stretching parameter. On the other hand, the x-domain must extend very far from the expansion in both directions where the outlet and inlet boundary conditions will be specified; however, the flow is expected to become smoother far from the expansion and the resolution necessary near the expansion is substantially more refined than far from it. We thus also introduce stretching of the x-axis by using the new coordinate η defined by

$$x = b\tanh^{-1}(\eta) + x_0. \tag{17}$$

In the new system of coordinates $\{\eta, \zeta\}$ a uniformly spaced rectangular grid is superimposed on the $(-1, 1) \times [0, 1]$ domain. Equations of motion are made discrete over such a grid by using centred second-order finite differences. At the two ends of the η-axis in the computational domain a simplified version of the equations is considered where only the second-order η-derivatives are set to zero. At the symmetry axis, $\zeta = 0$, and at the wall, $\zeta = 1$, conditions (7), (12), (13) hold. The right-hand side of (13) is evaluated by the first-order scheme discussed by Roache (1972). A second-order approximation has also been tested, giving no appreciable difference; the accuracy of the two methods is the same if, by symmetry considerations, the vanishing of odd derivatives of the streamfunction normal to the wall is assumed. The grid refinement near the wall introduced by (16) ensures a small truncation error. The independence of results from truncation is verified in the next section.

The nonlinear Jacobian term $\mathcal{J}(\omega, \psi)$ of the equation of motion is made discrete using the dealiased Arakawa (1966) scheme which guarantees the conservation of energy, circulation, and enstrophy (in unbounded two-dimensional flows) in the limit of vanishing viscosity. The equation of motion is integrated in time using the low-storage third-order Runge–Kutta scheme (Williamson 1980); the time step is chosen in order to guarantee the convective and diffusive stability conditions (Fletcher 1988).

The major time-consuming step in the integration procedure is the solution of the Poisson equation which corresponds to solving, three times per time step, a $(N_x \times N_r)^2$ linear system, where N_x and N_r are the number of grid points in the longitudinal and radial directions respectively. This linear system is, with the present choice of coordinates, made of nine diagonals, diagonal-dominant and non-symmetric. The solution is obtained by the bi-conjugate gradient-stabilized method (van der Vorst 1992), preconditioned with an incomplete LU decomposition (Meijerink & van der

Vorst 1981). This technique is simple to implement and has very rapid convergence characteristics even in stiff problems (Pedrizzetti & Novikov 1994). It leads, in the present application, to a computation complexity less than approximately $(N_x \times N_r)^{2.5}$ using convergence tolerance comparable with the machine precision. The whole code is run in double precision.

4. Oscillatory flow at $K_c = 50$, $\alpha^2 = 6$, $\delta = 1$

4.1. *Validation*

Once the numerical problem has been formulated we must define the appropriate computational resolution in order to obtain results which correspond to the physical problem. At present we have yet to define the grid stretching parameters a in the r-direction, b and x_0 in the x-direction; and the resolution $N_x \times N_r$.

During several tests, among which the experimental results of Ralph (1986, 1988) were reproduced with a version of the same code with a periodic-x boundary condition, a value for a of around unity has been found to be appropriate for the present order of magnitude of the diffusive term. In what follows we assume $a = 1.2$.

The distortion of the x-coordinate depends, in addition to the resolution, on the distance up to which the flow is significantly non-uniform. In order to define appropriate parameters we performed, with the present physical parameters, some short runs (up to $t = 5$) with the same resolution 192×36 (see below), with b ranging from 6 to 20 and x_0 from 0 to 8. It has been found that the non-uniformity in the flows dies out after a distance of about 30 radii from the expansion, and so the pair $b = 12$, $x_0 = 5$ is used in the calculation of the oscillatory flow.

Grid resolution has been checked by performing nine short runs (up to $t = 5$), using the stretching parameters specified above, with N_x ranging from 96 to 256 and N_r from 24 to 50. No significant difference could be found on varying radial resolution in this range and $N_r = 32$ has been chosen. In the x-direction a resolution $N_x = 192$ gives converged numerical results and will be used throughout the rest of the paper.

The flow forced by a periodic flow rate, has been found to be periodic in all cases presented below. The reference oscillatory case, and the pulsatile case of §6, were run for 100 periods revealing that a perfectly steady periodicity is established after an initial transient of about 4 periods. The results of all calculations present data extracted at the tenth period.

4.2. *Global features*

As the flow accelerates, a vortex sheet separates at the top of the expansion and rolls up forming a vortex ring. The vortex has a positive self-induced velocity and moves downstream, leaving the expansion. The instantaneous vorticity field is shown in figure 2 at every eighth of a period.

The self-induced velocity of the separated vortex ring is strong enough that the ring does not move backward during reverse flow and reaches a distance of about 10 radii downstream after one period. In the subsequent period the vortex continues its motion downstream and weakens so that, when the flow reverses, it is transported a small distance backward. Instantaneously the flow is then formed, in principle, by an array of vortex rings, weakening downstream, each one being generated in a successive flow oscillation; nevertheless, with the present choice of parameters, only two of them are of significant intensity while the previous ones have been dissipated by viscosity.

The presence of the vorticity in the bulk of the flow creates a persistent region of opposite vorticity at the wall that does not let the boundary layer follow the same

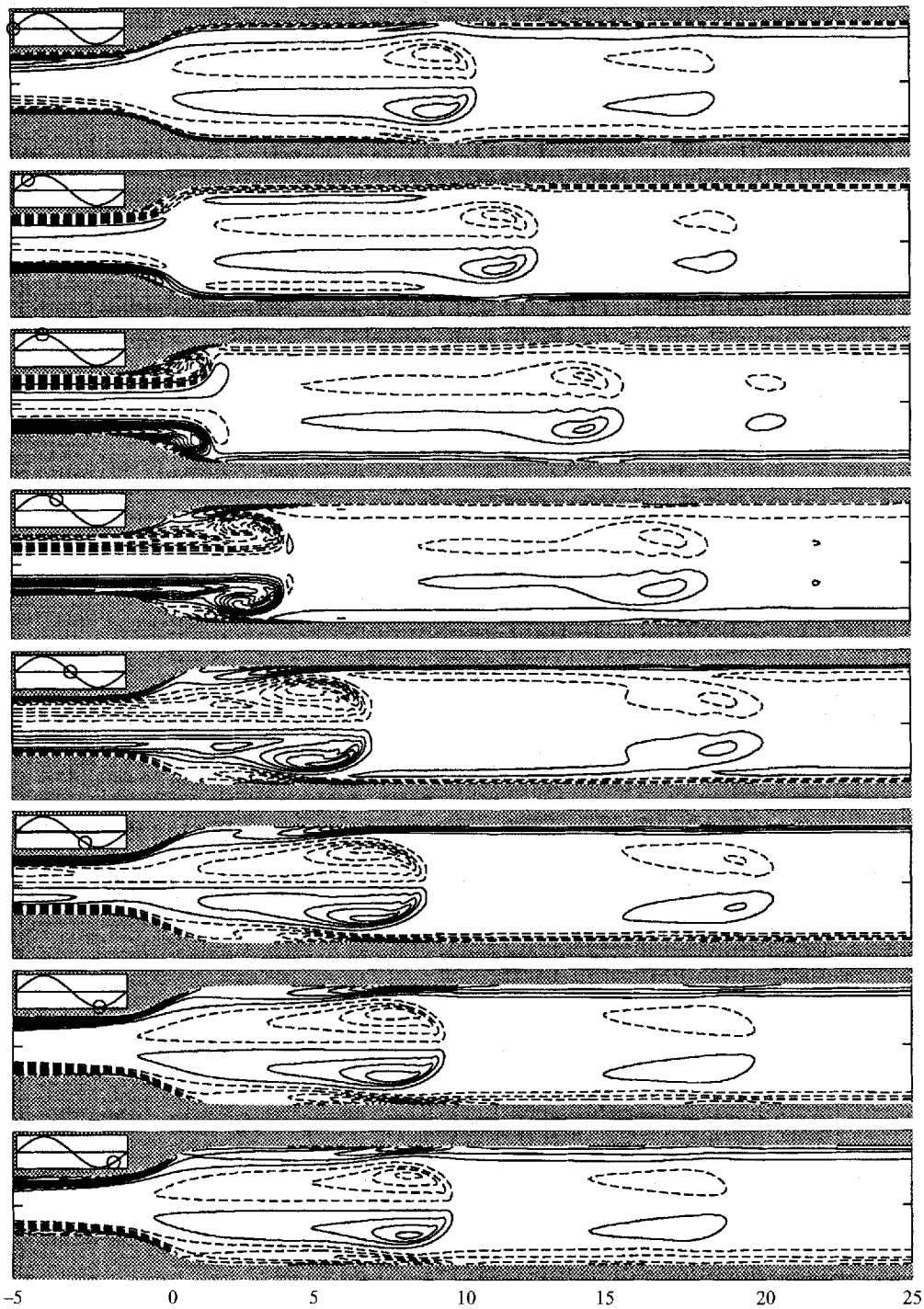

FIGURE 2. Vorticity contours for $\delta = 1$, $K_e = 50$, $\alpha^2 = 6$ from $t = 0$ every 1/8 of period. Levels from -410 to 410 in increments of 20. In this and subsequent similar figures positive levels are continuous lines, negative are dashed.

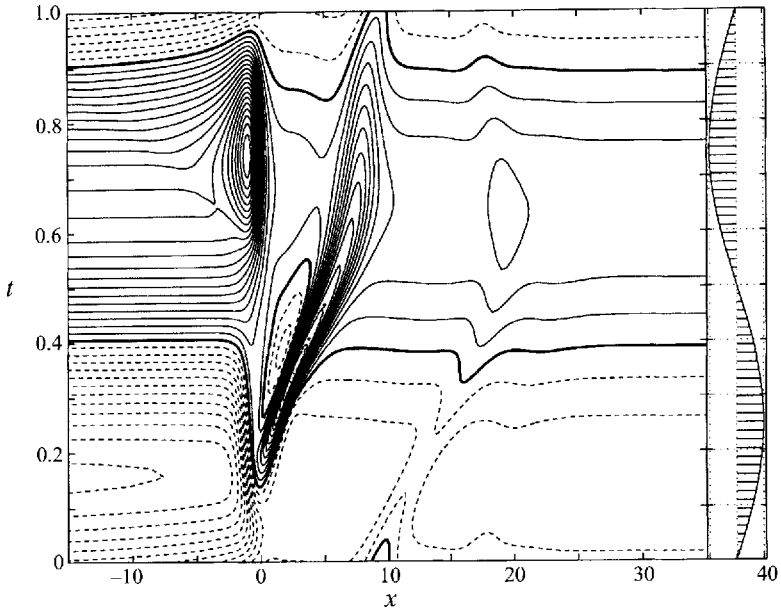

FIGURE 3. Wall shear stress contours in space–time for $\delta = 1$, $K_c = 50$, $\alpha^2 = 6$. Levels from -100 to 60, increment 5. The zero level is the thick continuous line, positive levels are dashed. Flow rate time variation is shown on the right.

oscillatory law as in a rectilinear duct (Batchelor 1967), which here can be observed only far downstream and upstream. The secondary vorticity at the wall does not separate and remains attached, creating a persistent negative wall shear stress.

Tangential stress at the wall can be computed from the definition of the stress tensor $\boldsymbol{T}$ in cylindrical coordinates (Batchelor 1967). Calling $\boldsymbol{\tau} = \boldsymbol{T}\cdot\boldsymbol{n}$ the stress vector, where $\boldsymbol{n}$ is the vector normal to the wall, the dimensionless wall shear stress is given by

$$\tau_w(x) = \frac{1}{\alpha^2}\omega(x, r = R(x)). \tag{18}$$

By analogy, the wall pressure is computed by integrating the pressure gradient along the wall as obtained by the Navier–Stokes equation in primitive variables which, in the present system of coordinates, leads to

$$p_w(x) = p_w(x_1) + \frac{1}{\alpha^2}\int_{x_1}^{x}\left[\frac{\mathrm{d}R}{\mathrm{d}x}\frac{\partial\eta}{\partial x}\frac{\partial\omega}{\partial\eta} - \frac{1+(\mathrm{d}R/\mathrm{d}x)^2}{R}\frac{\partial\zeta}{\partial z}\frac{\partial\omega}{\partial\zeta} - \frac{\omega}{R}\right]_{\zeta=1}\mathrm{d}x. \tag{19}$$

The development of the shear stress is relevant for the prediction of diseases in blood vessels (Pedley 1980). Figure 3 shows the space–time pattern of wall shear stress. On the right of the picture the time variation of the flow rate is shown for clarity.

Far from the expansion the shear stress changes sign in the same way as the oscillating flow in a rectilinear pipe. At $t \approx 0.15$ the separating vortex induces a negative stress at the expansion and at $t \approx 0.27$ secondary separation initiates a small zone of positive stress. The main feature is the trace of the separated vortex which, at the wall, marks a band of intense negative friction and extends with relevant intensity from separation up to the subsequent period. Overall, negative shear is substantially more prevalent than positive because of separation, and locally, can reach high values at about 1 to 8 radii from the expansion.

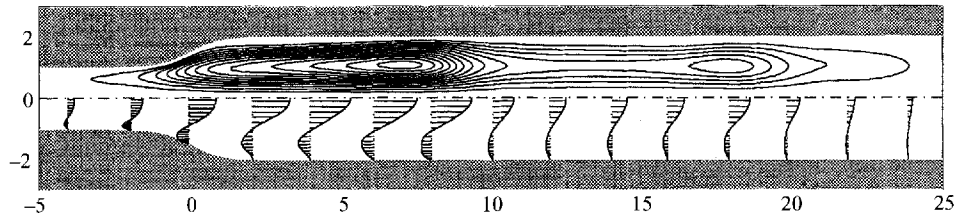

FIGURE 4. Cycle-averaged flow for $\delta = 1$, $K_c = 50$, $\alpha^2 = 6$. Upper half: streamfunction contours, levels from 0 to 6.5, increment 0.5. Lower half: velocity profiles, velocity units are reduced by a factor 0.06 with respect to spatial units.

The flow does not show the development of vortex waves as observed in previous two-dimensional simulations in channels with a sudden or gradual expansion (Sobey 1985; Tutty & Pedley 1993). In symmetric two-dimensional channels the analogy with the present results is negated by the symmetry breaking of the flow which occurs at Reynolds numbers of about 100 in steady flows (Durst, Pereira & Tropea 1993) and at smaller values in unsteady two-dimensional flows (Sobey 1985). A geometrical analogy could be drawn with the case of two-dimensional flow in a stepped channel, but the careful examination of the vortex wave development given by Tutty & Pedley (1993), even though their results are at a higher K_c ranging from 100 to 250, shows that these form by alternate deflection of the separated vorticity towards the two opposite no-slip walls with a fundamental role played by the induced separations, a phenomenon impossible in an axisymmetric geometry. Moreover, in two-dimensional flows the wake can bend more easily, whereas a resistance to such a curvature is intrinsically present in axisymmetric flow because it is accompanied by stretching of the annular vorticity and by increase of enstrophy.

4.3. *Cycle-averaged flow*

A non-zero value of the flow characteristics averaged over the cycle of zero mean indicates the presence of important nonlinear phenomena. This so-called 'steady streaming' is generated by the Reynolds stresses associated with the oscillatory shear layer (Schlichting 1968; Stuart 1963). In the present field the steady streaming extends from the inner layer and, by continuity, creates a mean recirculating flow. The steady pattern is shown in figure 4 (upper half) where the constant cycle-averaged streamfunction curves are plotted. On the lower half of the same picture the steady x-velocity profile confirms the single boundary layer structure of the steady streaming corresponding to a double vorticity layer structure. Keeping in mind the flow evolution shown in figure 2, we can observe that the steady streaming marks the regions in space associated with the persistence of the separated vorticity. Nonlinear terms are important in the separated parts of the flow, and in figure 4 we can recognize the average flow induced by the persistence of the separated vortex ring at $x \approx 7$, and the weaker vortex separated in the previous cycle at $x \approx 18$.

The presence of nonlinearity corresponds, in spectral terms, to the creation of additional harmonics superimposed on the fundamental one. The development of a second harmonic of frequency twice the fundamental one could be observed in almost all the flow field. Higher harmonics at discrete frequencies, multiples of the fundamental one, appear significantly just after the expansion. These appear also to be relevant at a large distance from the expansion about the mean position of the principal vortex, where energy is even larger at multiples than at the fundamental frequency, without any evident difference between odd and even harmonics. A similar behaviour with

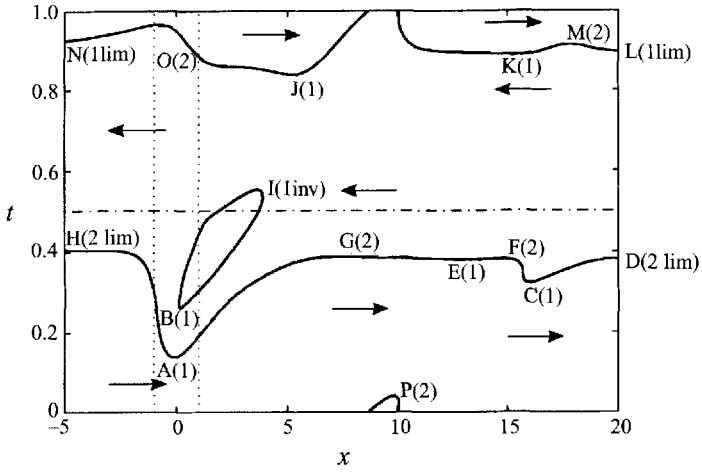

FIGURE 5. Zero-vorticity contour in space–time for $\delta = 1$, $K_c = 50$, $\alpha^2 = 6$. Arrows specify the direction of the wall limiting velocity; dotted lines indicate the step position; the dash-dot line indicates reversal of the flow. Letters denote limiting points and the associated number is their type (see text).

many excited harmonics in the vicinity of the farther vortex has been found in the different situation of oscillatory motion about a sphere (Chang & Maxey 1994) but no conclusion about similarities can be drawn at this stage.

4.4. *Separation*

Separation of the unsteady boundary layer gives rise to the large-scale vortex structures governing the flow development, and the understanding of some processes related to this has important implications in understanding and eventually predicting flow characteristics. For this reason we hope that a careful observation of the unsteady phenomena occurring near the wall can help in progressing this understanding and the classification of the unsteady separation mechanics.

The structure of the unsteady separation can be followed by looking at the critical points created at the no-slip wall. Critical points at the wall can be identified at each instant by zero limiting velocity, which is equivalent to zero vorticity. By using the linear approximation of the limiting velocity field near a critical point we can write (Perry & Fairlie 1974)

$$\frac{u}{\hat{y}} = \boldsymbol{A}\begin{bmatrix}\hat{x}\\ \hat{y}\end{bmatrix}, \tag{20}$$

where $\hat{y}$ denotes the distance from the wall and $\hat{x}$ denotes the distance from the critical point measured along the wall; the matrix $\boldsymbol{A}$ is given by (see also Perry & Fairlie 1974)

$$\boldsymbol{A} = \alpha^2\begin{bmatrix}\partial\tau_w/\partial\hat{x} & \frac{1}{2}\partial p_w/\partial\hat{x}\\ 0 & -\frac{1}{2}\partial\tau_w/\partial\hat{x}\end{bmatrix}, \tag{21}$$

where τ_w and p_w are given by equations (18) and (19). The top-left term indicates the intensity of the critical point and its sign indicates if it is a separating or a reattaching point; the top-right term indicates the tilt of the separating streamline with respect to the normal at the wall; the terms in the second row are a consequence of the continuity equation. Since the flow is planar, even if axisymmetric, all critical points are separating or reattaching saddles; of greater importance is their unsteady development during the oscillatory cycle.

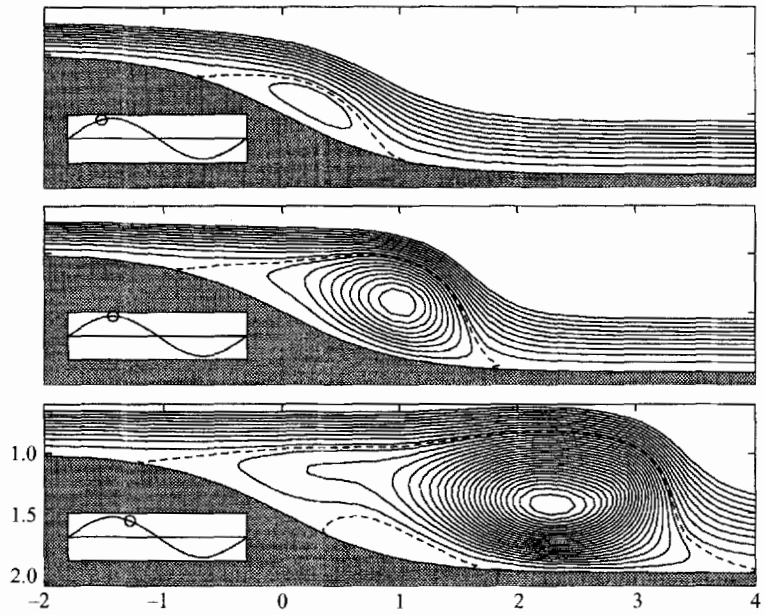

FIGURE 6. Streamlines for $\delta = 1$, $K_c = 50$, $\alpha^2 = 6$, at $t = 6/32, 8/32, 11/32$ from top to bottom. Levels from -7.6 to 20, increment 0.8 with respect to the instantaneous wall value, dashed line represents wall level.

In figure 5 the space–time evolution of the critical points at the wall is identified by plotting the zero-vorticity level; the arrows show the direction of the limiting velocity at the wall, dotted lines indicate the position of the expansion, and the dash-dot line marks the inversion of the mean flow. The letters, from A to P, indicate the position in space and time where a pair of saddles appears or disappears; these points are of particular relevance, being where separation starts or finishes, and we will call them *limiting points*. They are characterized by zero top-left and bottom-right terms in (21) leading to an instantaneously singular matrix $\boldsymbol{A}$. Two principal types of limiting points have been observed, as will be shown below; they are labelled as (1) and (2) in figure 5.

First, let us give a general picture of the separating dynamics as shown in figure 5. In a uniform tube, the limiting velocity is alternately positive and negative along the whole wall (Batchelor 1967; Schlichting 1968). In this axisymmetric case tube non-uniformity produces separation of vorticity. This induces a negative limiting velocity (A) and a secondary separation associated with positive limiting velocity (B); then a larger stress, due to the area reduction in reverse flow, results in the persistence of negative limiting velocity (O). These are the effects created directly by tube non-uniformity; these will then influence the rest of the flow. The separated vorticity moving forward because of self-induced velocity retards, with respect to oscillating flow in a uniform tube, the formation of positive vorticity at the wall underneath it, giving rise to limiting point P at the next cycle. The same vorticity, continuing its motion downstream, anticipates the formation of negative vorticity (C) and so on (M...). Secondary vorticity enters the flow at I and reattaches at J. Other smooth perturbations, like the one leading to the pair E F, may be attributed to different causes like the wake of the vortex ring.

The streamline pattern for the primary and secondary separation after the expansion is shown in figure 6. Primary separation, which develops from limiting point A, is

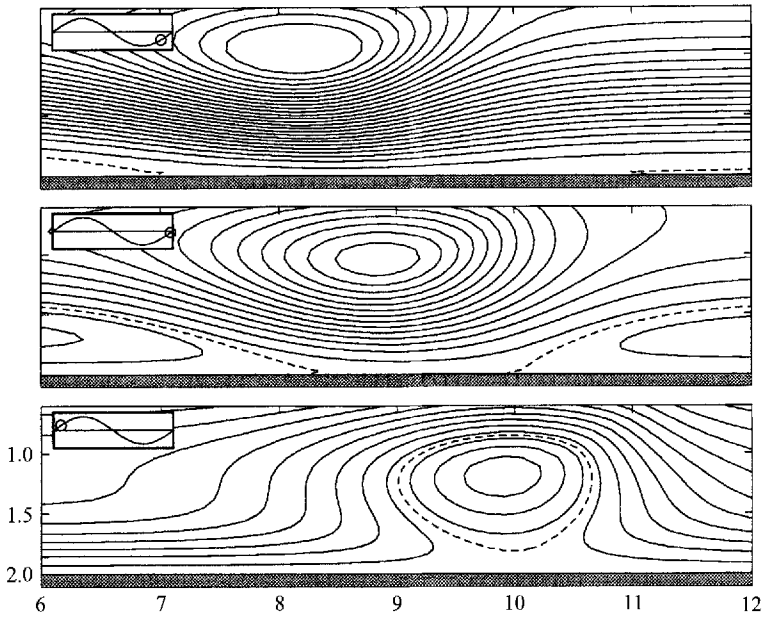

FIGURE 7. As figure 6 but at $t = 58/64$, $63/64$, $4/64$ from top to bottom.

typical of separation caused by a pressure gradient, developing as a growing recirculation cell. As the intensity of the bubble grows, because of the roll-up of the separated vorticity, it induces an opposite pressure gradient at the wall and a secondary separation contained inside the primary one appears (limiting point B). Both these limiting points can be seen as the appearance of one elliptic point at the wall (limiting points A and B) which then enters the flow giving rise to recirculation. This kind of limiting point is called type 1.

During decelerated motion a recirculation cell can progressively disappear. This is the case for the annihilation (limiting point I) of the secondary separation which can be interpreted as an inverse type-1 limiting point. More often, in the present results, different mechanics can be observed during deceleration motion. A recirculation attached to the wall is associated with limiting velocity in the opposite direction to the bulk flow; during deceleration and eventually reversal of the main stream the cell elongates, because limiting velocity of the same sign will eventually cover the whole wall, until it merges with an opposite saddle. In figure 7 we can see this process corresponding to the limiting point P. The separated cells, which appeared at J and K, elongate and exchange branches with neighbouring cells coming from L and N, then all the branches terminate in points M, O and P. The limiting point dynamics like that shown in figure 7 is classified as type 2. The main feature in this case is that the limiting point appears as a hyperbolic point at the wall which then enters the flow (it is worth noting, to avoid confusion, that the recirculation, or elliptic point, above the wall in figure 7 is not related to the wall limiting dynamics discussed here). This type of dynamics is related to the presence of non-uniform vorticity inside the flow; during deceleration vorticity at the wall wants to change sign but this process is also not uniform. In figure 7, the formation of positive wall limiting velocity is retarded below the vortex, which rotates clockwise. Limiting cases of both limiting points types arise when merging occurs with branches coming uniformly from infinity.

The a_{11} term in equation (21) for matrix $\boldsymbol{A}$ is zero at the limiting points. A typical type-1 separation (see point A, for example), induced by a positive pressure gradient, creates a recirculation cell with a negative shear stress gradient at the separating point and a positive one at reattachment. In such a case the limiting point is expected to present a positive pressure derivative and a positive second-order derivative of the tangential stress. The above result has been confirmed by the present calculation: we could see that when the a_{12} term is positive then the type-1 points are associated with a positive value of $\partial a_{11}/\partial \hat{x}$ and vice versa for negative values. On the other hand, given the sign of a_{12} and the sign of $\partial a_{11}/\partial \hat{x}$ then limiting points of type 2 correspond to opposite signs, revealing the dual nature of the different limiting point. This rule has also been confirmed by the results in the following sections. Such a rule may help in the development of the analytical treatment of unsteady separation (see, for example, the review article by Smith 1986 and references therein; and the recent developments by van Dommelen & Cowley 1990; Peridier *et al.* 1991) for planar flows.

4.5. *Pressure losses*

The value of pressure averaged over the pipe section, $p(x,t)$, is computed from the integral form of the momentum equation (Batchelor 1967; Marchi & Rubatta 1981) applied to a control volume confined by the tube wall and two tube sections at generic positions x_1 and $x > x_1$. Dropping the time dependence we can write

$$p(x) = p(x_1)\left(\frac{R(x_1)}{R(x)}\right)^2 + \mathscr{M}(x_1,x) + \mathscr{P}_t(x_1,x) + \mathscr{P}_n(x_1,x) + \mathscr{I}(x_1,x), \tag{22}$$

where the four operators on the right-hand side represent pressure variation due to, respectively, variation of momentum flux, tangential friction at the wall, normal pressure at the wall, and local inertia. They are given by

$$\left.\begin{aligned}
\mathscr{M} &= \frac{2}{R^2(x)}\left\{\int_0^{R(x_1)} u_x^2(x_1,r)\, r\,\mathrm{d}r - \int_0^{R(x)} u_x^2(x,r)\, r\,\mathrm{d}r\right\},\\
\mathscr{P}_t &= \frac{2}{R^2(x)}\int_{x_1}^{x} \tau_w(s)\, R(s)\,\mathrm{d}s,\\
\mathscr{P}_n &= \frac{2}{R^2(x)}\int_{x_1}^{x} p_w(s)\frac{\mathrm{d}R(s)}{\mathrm{d}s} R(s)\,\mathrm{d}s,\\
\mathscr{I} &= \frac{2}{R^2(x)}\frac{\mathrm{d}Q}{\mathrm{d}t}(x_1 - x).
\end{aligned}\right\} \tag{23}$$

The time evolution of the pressure jump between the sections at $x_1 = -10$ and $x = 20$ is shown in figure 8(*a*). Pressure difference (continuous line) and wall pressure difference (dotted) are almost coincident. Dashed lines are the contributions given by the different terms in equation (23). The total jump is dominated by the inertial term (P_n); the evolution is almost sinusoidal and is out of phase with the main stream.

An estimate of the pressure difference can be obtained by an inviscid analysis:

$$p(x) - p(x_1) = -\tfrac{1}{2}[R(x)^{-4} - R(x_1)^{-4}]\, K_c^2 f(t)\,|f(t)| - \int_x^{x_1} R^{-2}(s)\,\mathrm{d}s\, K_c \frac{\mathrm{d}f}{\mathrm{d}t}. \tag{24}$$

The first term on the right-hand side of equation (24) represents the kinetic

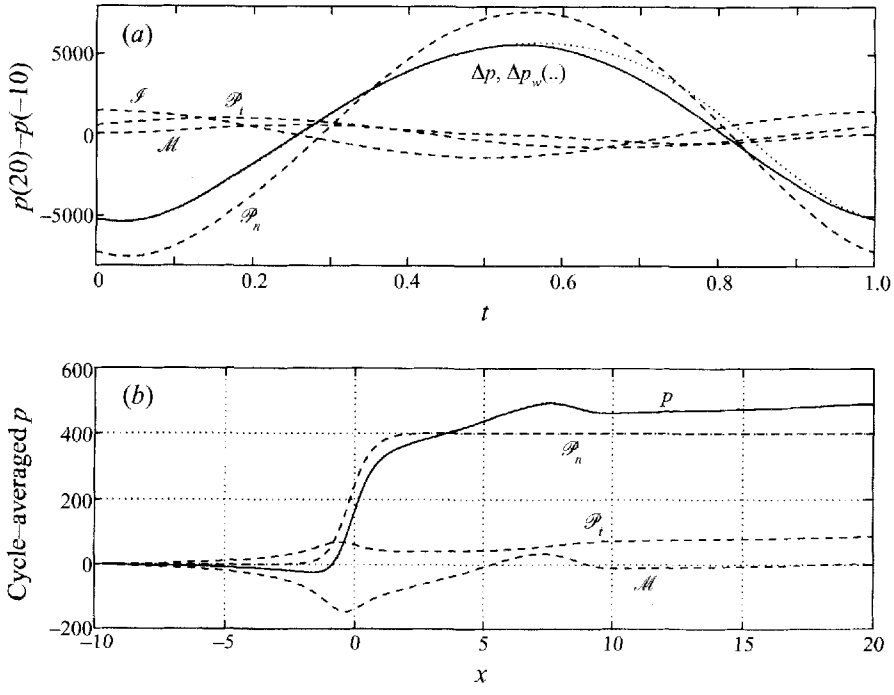

FIGURE 8. (*a*) Time evolution of the pressure difference, and (*b*) distribution along the tube of cycle-averaged pressure for $\delta = 1$, $K_c = 50$, $\alpha^2 = 6$.

contribution, and the second term is the inertial contribution. Equation (24) can be generalized to the Morison equation (de Bernardinis, Graham & Parker 1981; Bearman *et al.* 1985),

$$p(x) - p(x_1) = -C_d K_c^2 f(t)|f(t)| - C_m K_c \frac{\mathrm{d}f}{\mathrm{d}t}, \tag{25}$$

where the coefficients C_d and C_m can be obtained from (24). Actually the estimation of the drag coefficient C_d by equation (24) is rather poor because the approximation neglects dissipative phenomena related to separation. On the other hand the added-mass, or inertial term derives from bulk flow unsteadiness and equation (24) can give a rather good first approximation for C_m. A least-squares estimation of the coefficients in equation (25), with the data of figure 8, gives $C_d = 0.51$ and $C_m = 16.8$, whereas the inviscid estimate gives, respectively, -0.47 and 14.6.

The cycle-averaged pressure distribution along the tube is plotted in figure 8(*b*). The mean pressure difference is non-zero, as a consequence of the steady streaming. It is mainly due to wall pressure at the expansion, though some recovery is given by the contribution of the shear stress due to the recirculation seen in figure 4.

Formula (25) fails in representing the steady streaming contribution; however this is one order of magnitude smaller than the other contributions and has little influence in the case treated here and in the next sections. Approximation (25) represents the actual pressure variation with a relative error (root mean square of the error normalized with the root mean square of the pressure loss) below 15%. This estimate can be improved to 8% by subtracting the mean value. Notice that the drag term is substantially less important than the inertial term and the time variation of the pressure drop could be predicted from the inviscid estimate of the inertial term only, giving a relative error of 28%.

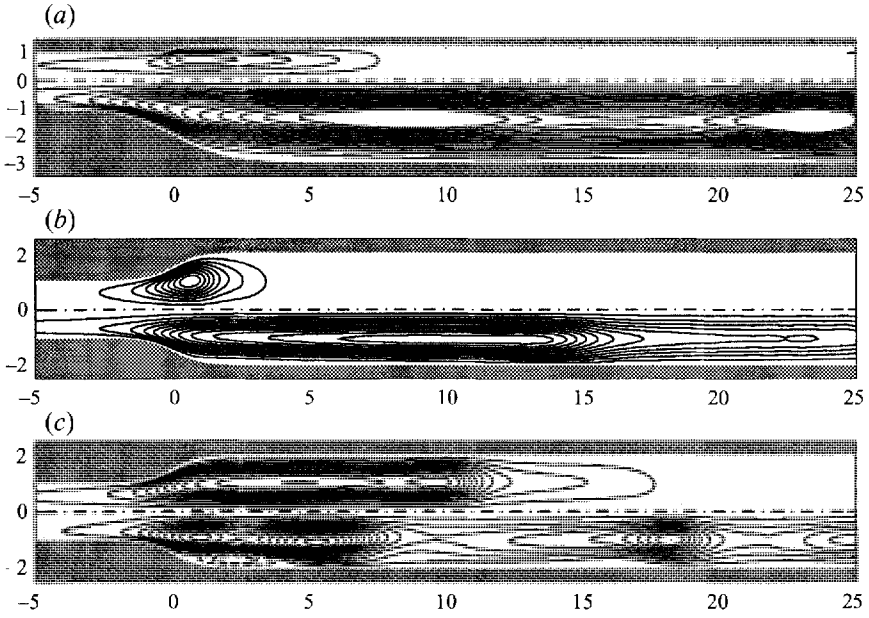

FIGURE 9. Cycle-averaged streamlines: (*a*) $\delta = 0.25$ (upper half) and 2 (lower half), $K_c = 50$, $\alpha^2 = 6$; (*b*) $\delta = 1$, $K_c = 15$ (upper half) and 75 (lower half), $\alpha^2 = 6$; (*c*) for $\delta = 1$, $K_c = 50$, $\alpha^2 = 3$ (upper half) and 12 (lower half). Levels from -1.25 to 7, increment 5.

5. Variation of flow parameters

5.1. *Expansion value* δ

In analogy with the finding by Tutty & Pedley (1993), the effect of decreasing the expansion is to decrease the intensity of the shed vortex rings. At values $\delta < 1$, the shed vortex travels a small distance beyond the duct enlargement and its motion is slowly backward during the reverse phase of the flow, indicating a smaller value of the self-induced velocity. A signature of the flow dependence on the parameter δ can be obtained by looking at the cycle-averaged streamlines. These are plotted in figure 9(*a*), at $\delta = 0.25$ and $\delta = 2$ in the upper half and lower half of the tube, respectively. Small δ creates a weak perturbation to the flow in the vicinity of the step which tends to zero on decreasing the step further. On the other hand a large value of δ creates a strong separated vortex which, as shown partially in figure 9(*a*), survives for more than two flow cycles. However the global behaviour does not change qualitatively from the reference case with $\delta = 1$. A typical mean position of the separated vortex can be extrapolated from the position of the maximum value of the averaged streamfunction, as shown in figure 9(*a*); such an estimation gives $x = 0.8, 3.6, 7.1, 8.8$ for $\delta = 0.25, 0.5, 1, 2$, respectively. The structure of separation analysed in the previous section is maintained even through secondary separation does not occur for $\delta = 0.5$. The unsteady pressure drop can still be expressed by the Morison equation (25); the growth of the inertial contribution with δ is in agreement with the inviscid estimate (24) which give C_m ranging from about 23 to 11 with growing expansion height.

5.2. *Keulegan–Carpenter number* K_c

The Keulegan–Carpenter number represents the ratio between the length of the free-stream oscillation and the reference length scale. In this view and in dimensionless terms, K_c can be interpreted as a longitudinal length scale of flow motion. The primary effect of its variation is to elongate, or shorten, the influence of non-uniformity in the

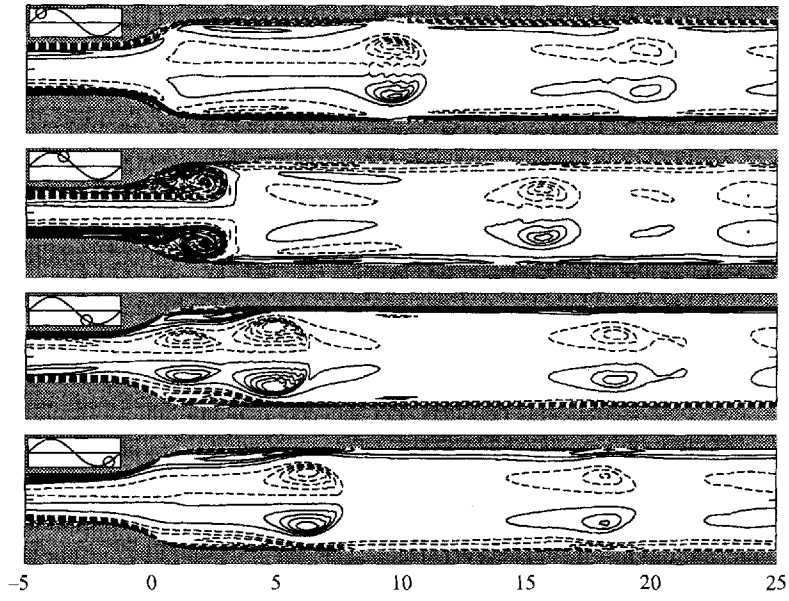

FIGURE 10. Vorticity contours for $\delta = 1$, $K_c = 50$, $\alpha^2 = 12$ from $t = 1/8$ every 1/4 period. Levels from -510 to 510, increment 20.

tube. This can be seen in figure 9(*b*), where the steady streamlines are shown for $K_c = 15$ (upper half of the tube) and $K_c = 75$ (lower half). The elongation of the wake grows approximately linearly with K_c, though the limitation in the range of variation means that we cannot consider such a conclusion as definitive.

For large enough values of K_c, larger than the small dimensionless length scales given by the diffusion length and expansion size, there is no other longitudinal length scale which can compete with the wake development. Consequently the flow is expected to extend, in a fashion similarity, with no limitation. This is in agreement with previous results for flow over an expansion (Sobey 1985; Tutty & Pedley 1993). The results are different, as expected, when an additional length scale such as the wavelength of a periodic wall non-uniformity, is present. This is the case of flow over a rippled bed (Blondeaux & Vittori 1991*a*) and flow in a wavy walled tube (Ralph 1986) who found a resonating value of the Strouhal number corresponding to oscillations comparable with wall wavelength. In that case the interaction of wakes shed from neighbouring crests can lead to complex, possibly chaotic (Blondeaux & Vittori 1991*b*) vortex dynamics, whereas in the present case separated vortices do not come close enough to develop any intense interaction.

5.3. *Stokes parameter* α^2

The parameter α^2 represents the inverse, squared, of the thickness of the boundary layer with respect to the inlet radius. In figure 9(*c*) steady streamlines are shown for $\alpha^2 = 3$ and $\alpha^2 = 12$. Small values of α^2 correspond to a viscous smooth separated vortex. Larger values correspond to a weaker diffusive effect and, as a consequence, induce a thinner boundary layer and separated vortex sheet and longer-living vortices; a double boundary layer structure is clearly seen at the foot of the expansion for $\alpha^2 = 12$ (this had already appeared for $\alpha^2 = 9$) reflecting the smaller thickness of the boundary layer. In figure 10 the vorticity field is shown, for $\alpha^2 = 12$, at four equispaced instants. At the end of the flow acceleration the thin vortex sheet rolls up into one compact vortex. This induces a relatively intense secondary separation which, trying to

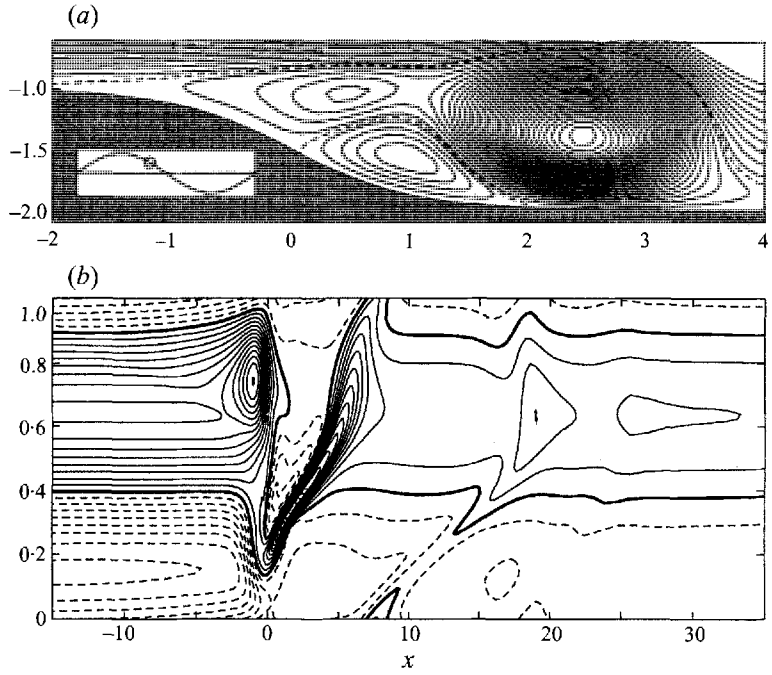

FIGURE 11. Wall flow for $\delta = 1$, $K_c = 50$, $\alpha^2 = 12$. (*a*) Streamlines at $t = 13/32$, levels from -7.6 to 30, increment 0.8 with respect to the instantaneous wall value; dashed line represents wall level. (*b*) Wall shear stress contours in space–time, levels from -100 to 60, increment 5.

separate itself, is able to isolate the vortex from the remainder of the separating vorticity which organizes into another weaker patch following the primary vortex.

The separation dynamics is globally similar to the reference case of §4 with a noticeable difference in the secondary separation. This is summarized in figure 11 where, upper picture, instantaneous streamlines at approximately the maximum growth of secondary separation and, lower picture, wall shear stress space–time development are reported. Secondary separation penetrates inside the flow and creates two primary recirculating cells. The wall stress evolution shows that secondary separation is not extinguished during flow reversal but maintains a positive shear at the foot of the expansion until the appearance of primary separation in the next flow cycle. It can also be noted that the intensity of the secondary vorticity at the wall presents a bifurcation at flow reversal, indicating a possible tertiary separation at larger α^2 values.

6. Pulsatile flow

In this section we analyse the flow arising from a time law variation of the fluid volume rate inside the tube of the same type as those observed in large arteries of human circulation systems. The analysis is along the same lines as for the previous cases and the main differences with the case of purely sinusoidal unsteady flow rate are explored. Flow parameters are the same as in §4.

Approximating several actual Doppler measurements in the human carotid artery we found that the function

$$\begin{aligned} f(t) = {} & 0.4355 + 0.05\cos(2\pi t) + 0.25\sin(2\pi t) - 0.13\cos(4\pi t) \\ & + 0.13\sin(4\pi t) - 0.10\cos(6\pi t) - 0.02\sin(6\pi t) \\ & - 0.01\cos(8\pi t) - 0.03\sin(8\pi t) \end{aligned} \tag{26}$$

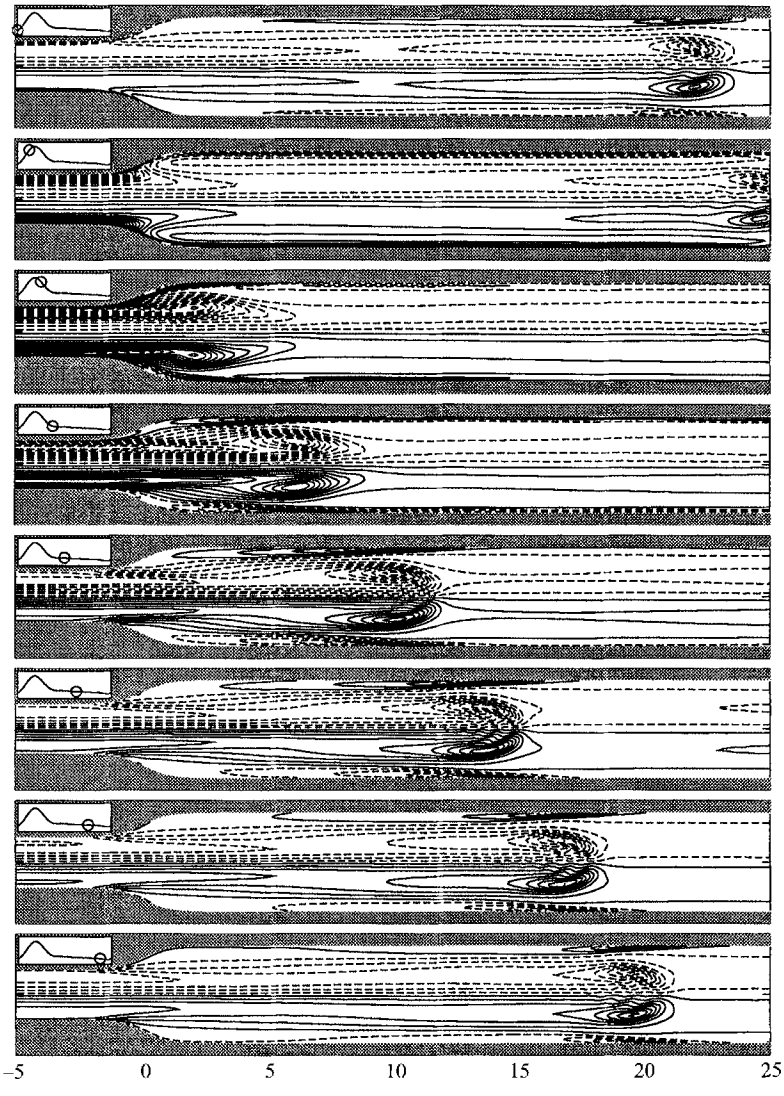

FIGURE 12. Vorticity contours in pulsatile flow for $\delta = 1$, $K_c = 50$, $\alpha^2 = 6$ from $t = 0$ every 1/8 period. Levels from -155 to 335, increment 10.

represents a simple good approximation of the real flow time evolution. Law (26) does not include flow reversal and is composed, in each period, of an impulsive motion with strong acceleration and deceleration (systole) followed by a slowly decelerating flow. It reaches the maximum value of unity at about $t = 0.18$, and the mean values is 0.4355.

The presence of a positive mean flow rate implies the necessity to extend the computational domain further downstream. Several tests varying the parameters b and x_0 and grid size N_x have been performed in analogy with §4. It could be verified that a better representation of the flow to far downstream is achieved assuming $b = 16$ and $x_0 = 8$ while keeping the other parameters unchanged.

The vorticity field during one pulsation is shown in figure 12; pictures are plotted every eighth of a period. A vorticity wake is created during the impulsive phase which rolls up into a well-defined vortex structure at the end of the rapid deceleration phase, as can be observed in the fourth frame of figure 12. The separated vortex ring moves

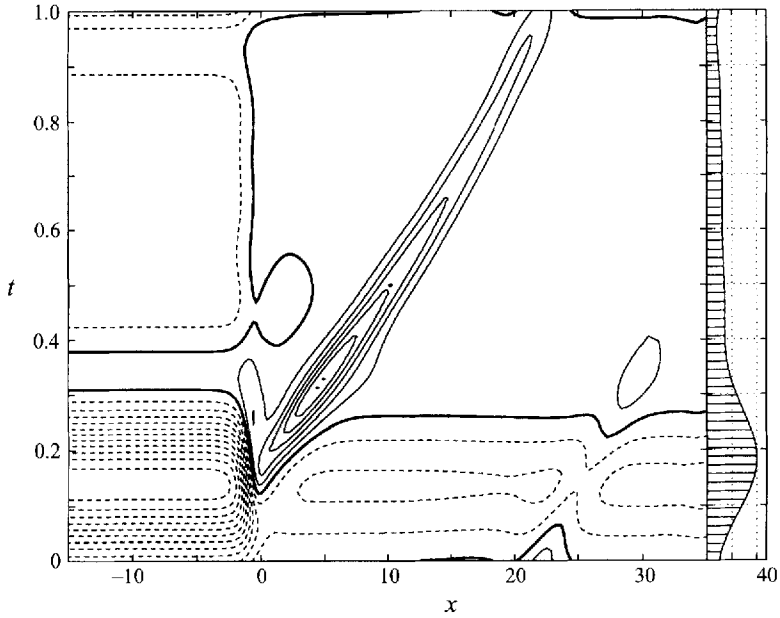

FIGURE 13. Wall shear stress contours in space–time in pulsatile flow for $\delta = 1$, $K_c = 50$, $\alpha^2 = 6$. Levels from -100 to 60, increment 5. Flow rate time variation is shown on the right.

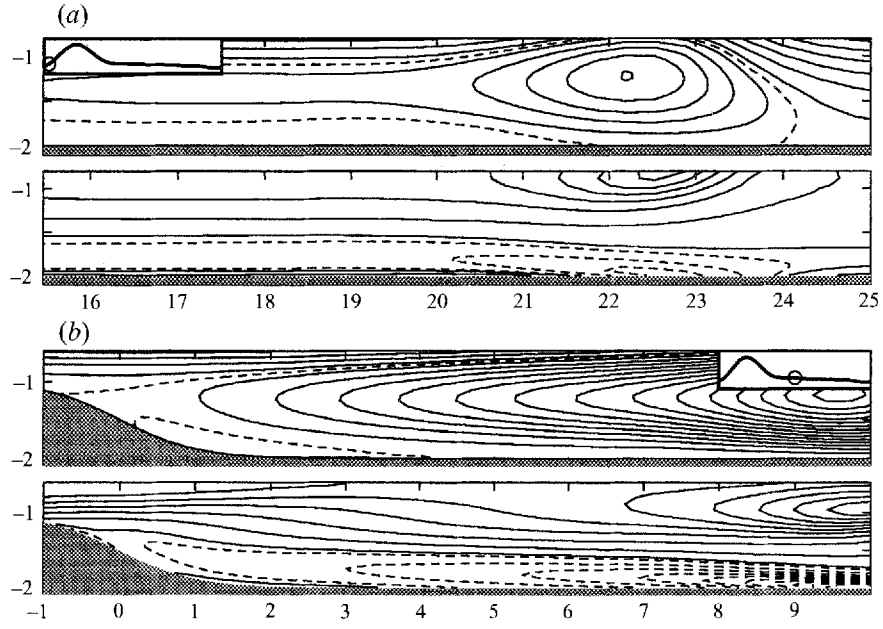

FIGURE 14. Streamlines (above) and vorticity (below) in pulsatile flow for $\delta = 1$, $K_c = 50$, $\alpha^2 = 6$, at (*a*) $t = 1/32$, (*b*) 16/32. Streamfunction levels from -7.6 to 20, increment 0.8 with respect to the instantaneous wall value; dashed line represents wall level; vorticity levels from ± 2 with increment 10.

downstream because of the self-induced motion and the positive flow rate. The sequential separation of a vortex ring every time cycle results in a succession of vortices, weakening downstream, which are spaced further apart than in the purely oscillatory case. With the present choice of physical parameters, the vortex propagates

downstream up to a distance of about 40 inlet radii. As observed in the oscillatory case, a secondary vorticity layer is maintained at the wall underneath the primary vortex. The space–time development of the wall shear stress is shown in figure 13. As the flow is always directed toward the larger portion of the tube the dominance of positive wall shear is expected and the only noticeable negative shear is that induced below the primary vortex. Significant positive shear can be observed during all the impulsive phase, decreasing to about zero throughout the phase of slow deceleration; similar behaviour at the wall can be seen in the results for pulsatile two-dimensional flow beyond constriction presented by Tutty (1992).

The cycle-averaged flow is qualitatively similar to what is obtained in steady flow even though the recirculation cell is slightly more intense and its elongation downstream increases from about 20 to 24 units. The separation features are similar to the oscillatory flow (see figure 13) with analogous appearances of the principal limiting points. The extinguishing of the negative shear below the major vortex is shown in figure 14(*a*), where streamlines (above) and vorticity contours (below) correspond to $t = 0.031\,25$. Negative vorticity is lifted because acceleration encourages positive shear to develop along the wall giving rise to a type-2 limiting point disappearance (compare with figure 7). Secondary separation appears at the foot of the expansion during deceleration with a type-1 limiting point at $t \approx 0.39$. The recirculating cell connects with the positive limiting velocity coming from infinitely far upstream at a type-2 limiting point, and is recreated with an inverse type-2 limiting point, reaching the stage shown on figure 14(*b*).

The pressure difference through the expansion is still dominated by the inertial effect. The difference between wall pressure and mean pressure is below 1% here, due to the dominance of longitudinal velocity. On average, in a cycle, the distribution of pressure along the tube is very similar to what is obtained in steady flow with a slightly larger recovery and final smaller pressure loss. The Morison equation (25) gives a very good representation of the temporal evolution of the pressure drop with coefficients $C_d = 0.13$ and $C_m = 16$ (error 6%); a prediction of pressure drop from the inertial term of the inviscid estimate (24) results in an approximation with relative error below 12%.

7. Conclusions

Unsteady flow in a circular channel with a smooth expansion has been analysed with the approximation of axial symmetry of the flow. The major large-scale feature in oscillatory flow is the formation of a train of vortex rings, each formed during one oscillation cycle. Variation of the step height and of the Keulegan–Carpenter number only influences the strength and the elongation of the separated vorticity without modification of the general picture. Variation of the Stokes number has shown that a vorticity patch with two maxima, or eventually a pair of vortices, can separate each cycle. Steady streaming, revealing the nonlinear character of separated flows, is found in all cases with a single boundary layer structure; a double layer structure is found at larger Stokes number, corresponding to the double maxima separated vortex. Most of the experimental and numerical results for the similar problem of oscillatory flow after a step have been developed in a two-dimensional flow model. The development of vortex waves observed in several studies and in a different geometry (Sobey 1985; Tutty 1992; Tutty & Pedley 1993) could not be observed in axisymmetric dynamics because they are related to the presence of two facing no-slip walls (Tutty & Pedley 1993).

Moreover, radial motion of vorticity is made more difficult in axisymmetric flows because of its association with the stretching of circular vortex lines.

In unsteady flows with a sequence of accelerated and decelerated, eventually reversing, flow, the definition of separating and reattaching points can sometimes be misleading because these definitions intrinsically refer to the direction of the flow above the wall. A space–time view of the limiting flow at the wall has revealed some features of the separating dynamics. Two dual dynamics for the appearance and disappearance of pairs of critical points at the wall could be recognized by the present calculations. The major feature, common in all calculations, is the development of a negative wall shear stress region induced by the separated vortex ring and moving along with it in the expanded portion of the tube.

The difference between the values of the pressure before and after the expansion is dominated by the inertial contribution. The absence of a longitudinal length scale, which could compete with the oscillation length, reduces the possibility of an interaction between vortices of comparable intensity and the consequent cascade to complex dynamics as observed in a wavy-walled tube (Ralph 1986, 1988). For this reason the time development of pressure differences is substantially represented by the flow rate time derivative, and can be predicted to a good approximation by the inertial contribution of an inviscid flow analysis. Nonlinearity appears more significant for increasing values of the Stokes parameter, indicating a possible source of complex dynamics. At these large values the axisymmetric flow is presumably unstable and the present results can be a reference starting point for three-dimensional flow analysis.

This work was stimulated by the need to understand the fluid dynamical phenomena corresponding to post-surgical carotid conditions. Even though the flow at this site is certainly three-dimensional due to bifurcation of the artery's wall a few radii after the expansion, and the elasticity of the walls can have a fundamental influence in the flow development, the flow associated with a pulsatile fluid volume rate has been considered in order to explore the findings which can be obtained with the present idealized model. The qualitative flow development is substantially similar to the oscillatory case even though quantitative differences, like the spacing between successive separated vortices, are relevant. Pressure losses are, on average, smaller than in steady flows but instantaneous peaks can be more than one order of magnitude larger. These can be predicted to a good approximation (error around 10%) by the inviscid estimate of the inertial term.

The development of shear stress at the wall, and its space–time pattern, is of particular relevance for the localization and prediction of arterial diseases. During the reverse phase of oscillatory flow negative wall shear stress is distributed along the whole tube wall with one maximum at the top of the expansion and another one at the wall which are induced by the separated vortex moving inside the channel. In the pulsatile case intense negative shear is almost absent during the whole period apart from at the wall in the neighbourhood of the main vortex. Its space–time development indicates that a relevant portion of the tube, from the expansion to about 20 inlet radii downstream, is subjected to an oscillatory stress even in pulsatile flow, with large negative peaks. This phenomenon differs from the vortex waves observed past a two-dimensional expansion, but appears to have some generality in axisymmetric geometry.

The author acknowledges the use of the computational facilities of PIN at Prato (teaching and scientific services for the University of Firenze).

REFERENCES

ARAKAWA, A. 1966 Computational design for long term numerical integration of the equation of fluid motion: two dimensional incompressible flow. Part I. *J. Comput. Phys.* **1**, 119–143.

BATCHELOR, G. K. 1967 *An Introduction to Fluid Dynamics*. Cambridge University Press.

BEARMAN, P. W., DOWNIE, M. J., GRAHAM, J. M. R. & OBASAJU, E. D. 1985 Forces on cylinders in viscous oscillatory flow at low Keulegan-Carpenter numbers. *J. Fluid Mech.* **154**, 337–356.

BERNARDINIS, B., DE, GRAHAM, J. M. R. & PARKER, K. H. 1981 Oscillatory flow around disks and through orifices. *J. Fluid Mech.* **102**, 279–299.

BLONDEAUX, P. & VITTORI, G. 1991*a* Vorticity dynamics in an oscillatory flow over a rippled bed. *J. Fluid Mech.* **226**, 257–289.

BLONDEAUX, P. & VITTORI, G. 1991*b* A route to chaos in an oscillatory flow – Feigenbaum scenario. *Phys. Fluids* A, **3**, 2492–2495.

CHANG, E. J. & MAXEY, M. R. 1994 Unsteady flow about a sphere at low to moderate Reynolds number. Part 1. Oscillatory motion. *J. Fluid Mech.* **277**, 347–379.

DURST, F., PEREIRA, J. C. F. & TROPEA, C. 1993 The plane symmetric sudden-expansion flow at low Reynolds numbers. *J. Fluid Mech.* **248**, 567–581.

EISEMAN, P. R. 1985 Grid generation for fluid mechanics computation. *Ann. Rev. Fluid Mech.* **17**, 487–522.

ERSOY, S. & WALKER, J. D. A. 1987 The boundary layer due to a three-dimensional vortex loop. *J. Fluid Mech.* **185**, 569–598.

FLETCHER, C. A. 1988 *Computational Techniques for Fluid Dynamics I*. Springer.

JUSTENSEN, P. 1991 A numerical study of oscillating flow around a circular cylinder. *J. Fluid Mech.* **222**, 157–196.

MARCHI, E. & RUBATTA, A. 1981 *Meccanica dei Fluidi*. UTET Torino.

MEI, R. & ADRIAN, M. J. 1992 Flow past a sphere with an oscillation in the free-stream velocity and unsteady drag at finite Reynolds number. *J. Fluid Mech.* **233**, 613–631.

MEIJERINK, J. A. & VORST, H. A., VAN DER 1981 Guidelines for the usage of incomplete decompositions in solving sets of linear equations as they occur in practical problems. *J. Comput. Phys.* **44**, 134–146.

NAKANO, M. & ROCKWELL, D. 1994 Flow structure in the frequency modulated wake of a cylinder. *J. Fluid Mech.* **266**, 93–119.

PEDLEY, T. J. 1980 *The Fluid Mechanics of Large Blood Vessels*. Cambridge University Press.

PEDLEY, T. J. & STEPHANOFF, K. D. 1995 Flow along a channel with a time-dependent indentation in one wall: the generation of vortex waves. *J. Fluid Mech.* **160**, 337–367.

PEDRIZZETTI, G. 1992 Close interaction between a vortex filament and a rigid sphere. *J. Fluid Mech.* **245**, 701–722.

PEDRIZZETTI, G. & NOVIKOV, E. A. 1994 On Markov modelling of turbulence. *J. Fluid Mech.* **280**, 69–93.

PERIDIER, V. J., SMITH, F. T. & WALKER, J. D. A. 1991 Vortex-induced boundary-layer separation. Part 1. The unsteady limit problem $Re \to \infty$. *J. Fluid Mech.* **232**, 99–131.

PERRY, A. E. & FAIRLIE, B. D. 1974 Critical points in flow pattern. *Adv. Geophys.* **18 B**, 299–315.

RALPH, M. E. 1986 Oscillatory flow in wavy-walled tubes. *J. Fluid Mech.* **168**, 515–540.

RALPH, M. E. 1988 Pressure drop and power dissipation in oscillatory wavy-walled tube flows. *J. Fluid Mech.* **187**, 573–588.

RALPH, M. E. & PEDLEY, T. J. 1988 Flow in a channel with a moving indentation. *J. Fluid Mech.* **190**, 87–112.

RALPH, M. E. & PEDLEY, T. J. 1989 Viscous and inviscid flows in a channel with a moving indentation. *J. Fluid Mech.* **209**, 543–566.

ROACHE, P. J. 1972 *Computational Fluid Dynamics*. Hermosa.

SCHLICHTING, H. 1968 *Boundary-Layer Theory*, 6th edn. McGraw-Hill.

SMITH, F. T. 1986 Steady and unsteady boundary layer separation. *Ann. Rev. Fluid Mech.* **18**, 197–220.

SOBEY, I. J. 1985 Observation of waves during oscillatory channel flow. *J. Fluid Mech.* **151**, 395–426.

STUART, J. T. 1963 Unsteady boundary layers. In *Laminar Boundary Layers* (ed. L. Rosenhead). Oxford University Press.

TATSUNO, M. & BEARMAN, P. W. 1990 A visual study of the flow around an oscillating circular cylinder at low Keulegan-Carpenter numbers and low Stokes numbers. *J. Fluid Mech.* **211**, 157–182.

TUTTY, O. R. 1992 Pulsatile flow in a constricted channel. *J. Biomech. Engng* **114**, 50–54.

TUTTY, O. R. & PEDLEY, T. J. 1993 Oscillatory flow in a stepped channel. *J. Fluid Mech.* **247**, 179–204.

VAN DOMMELEN, L. L. & COWLEY, S. J. 1990 On the Lagrangian description of unsteady boundary-layer separation. Part 1. General theory. *J. Fluid Mech.* **210**, 593–626.

VORST, H. A., VAN DER 1992 BiCGSTAB – A fast and smoothly converging variant of Bi-CG for the solution of nonsymmetric linear systems. *SIAM J. Sci. Statist. Comput.* **13** (2), 631–644.

WILLIAMSON, J. H. 1980 Low-storage Runge–Kutta schemes. *J. Comput. Phys.* **35**, 48–56.